Journal of AI and Data Mining
Vol 6, No 1, 2018, 13-33

Image Restoration by Variable Splitting based on Total Variant Regularizer

E. Sahragard [1], H. Farsi [1*] and S. Mohamadzadeh[2]

1. Department of Electrical & computer Engineering, University of Birjand, Birjand, Iran
2. Faculty of Technical & Engineering Ferdows, University of Birjand, Birjand, Iran.

Received 22 November 2015; Revised 05 November 2016; Accepted 19 May 2017
**Corresponding author: hfarsi@birjand.ac.ir (H. Farsi).*

Abstract
The aim of image restoration is to obtain a higher quality desired image from a degraded one. In this strategy, an image inpainting method fills the degraded or lost area of the image by an appropriate information. This is achieved in such a way that the image obtained is undistinguishable for a casual person who is unfamiliar with the original image. In this work, different images are degraded by two procedures; one is to blur and to add noise to the original image, and the other one is to lose a percentage of the original image pixels. Then the degraded image is restored by the proposed method and also two state-of-art methods. For image restoration, it is required to use the optimization methods. In this work, we use a linear restoration method based upon the total variation regularizer. The variable of optimization problem is split, and the new optimization problem is then solved using the Lagrangian augmented method. The experimental results obtained show that the proposed method is faster, and the restored images have a higher quality compared to the other methods.

Keywords: *Image Restoration, Image Inpainting, Deblurring, Total Variation Regularizer, Lagrangian Augmented.*

1. Introduction

Image restoration is known as one of the most important image processing techniques. It is used in various applications and areas such as medical, astronomical imaging, image and video coding, remote sensing, military, seismography, aerology, and film restoration [1]. In space exploration, the image restoration systems have been used by researchers since 1960 [2]. Providing the desired image from the degraded one is the aim of the image restoration systems. An image restoration system contains de-blurring, de-noising, and preserving fine details [3]. The information and details of the image are lost when the image is captured. The restoration not only removes the noise of images but also is widely used in blind deconvolution, image inpainting, and various image processing methods [4, 6].

Image restoration may contain several applications such as blind deconvolution, image deblurring, image inpainting, and image denoising. For each application, a special method is used for image degradation and restoration. This paper focuses on image inpainting and deblurring. The image inpainting is a process of reconstructing the corrupted or lost parts of the image that is undistinguishable for a casual person who is unfamiliar with the original image. The image inpainting plays an important role in various image processing applications such as removal of scratches in old photographs and videos, filling in missing blocks in unreliably transmitted images, and removal of overlaid text or graphics [5]. Image demolition is caused by a non-adjusted camera, object and camera motion, reflection from uncontrollable sources, and non-ideal photographic and communication systems [5]. The most common problems involved in photography are the image blurring and noise. The blurring occurs due to a localized averaging of pixels, and significant in light limited situations and resulting in a ruined photograph. Image deblurring is the process of recovering a sharp image from a corrupted one. The blurring contains environmental blurs and motion blurs.

The reason for the environmental blurs is a light passing through the media environment with different refractive indices. The motion blurs are caused by the relative motion between a camera and a scene [7]. In this paper, we assumed that the motion blurs were distinguishable and estimable, and that the noise was Gaussian distribution with zero mean. The image restoration system includes three important parts: a) modelling the degraded image, b) formulating the image restoration problem, and c) designing an efficient and accurate method in order to solve the image restoration problem.

In the modelling part, the blurring and noise information is used to create a model of the degraded image. In many recent research works, a linear model is used to model the degraded image. Common degradations include noise, blurring, color imperfections, and geometrical distortions. The image restoration problems can be modeled using the following expressed linear degradation model:

$$y = Bx + n, \tag{1}$$

where, B is a Point Spread Function (PSF), x is the original image, n is the noise matrix, and y represents the degraded image. Note that PSF is the degree to which an optical system blurs (spreads) a point of light. PSF is the inverse Fourier transform of Optical Transfer Function (OTF) in the frequency domain. OTF describes the Response of a linear, position-invariant system to animpulse. OTF is the Fourier transfer of the point (PSF). If PSF is specified (PSF is the same for all image pixels), Equation (1) indicates the deconvolution problem, otherwise it presents the blind deconvolution problem.

Blind Image Restoration: This technique allows the reconstruction of original images from the degraded ones even when a little or no knowledge is available about PSF. Blind Image Deconvolution (BID) is an algorithm of this type [22].

Non-Blind Restoration: This technique aids in the reconstruction of original images from the degraded ones when the process of image degradation is known, which means that the PSF information is available [22].The image restoration problem is more accurately expressed using a non-linear regularizer. Therefore, in this work, it was tried to use this regularizer. In (1), x and y indicate the original and degraded images, respectively, and B is a linear operator that represents a blur matrix in case of blurring image or losing a number of image pixels in case of inpainting image. In order to construct the degraded image, it is required to add the linear operator of B and noise to the original image. Depending upon the linear operator, B, which includes the blur or the lost pixels, the image restoration problem will differ. If B contains the blur, the image restoration problem changes to the deblurring, and if B indicates the lost pixels, it converts to the inpainting.

In the formulating part, the information for the degraded and original images is used to formulate the objective function and then to remove the noise and blurring from the degraded image. This function is solved using the inverse function or optimization problem. The image restoration problem that is solved by convex optimization uses unconstrained optimization, as follows:

$$\min_{x} \frac{1}{2}\|y - Bx\|_2^2 + \tau\phi(x), \tag{2}$$

where, $\|.\|_p$ is p-norm, and is given by:

$$\|A\|_p = \left(\sum_{i=1}^{n} |a_i|^p\right)^{1/p} \tag{3}$$

where, n is the number of matrix element *A* after reshaping.

The optimization problem contains two parts: data fidelity and smooth regularizer. In a practical research work, the regularizer is completely unable to model the characteristic of the original image. Therefore, we should compromise between the regularizer and the data fidelity. For instance, in figure 1(a), the cameraman image is degraded by the 9*9 uniform blur and additive Gaussian noise with zero mean. Figure 1(b) shows that the regularizer has a small effect, and the output noise is amplified for a very small regularizer parameter ($\tau = 0.001$). On the other hand, figure 1(C) shows that the large regularizer parameter ($\tau = 10$) provides a much smoothed image and removes the edges of image. Thus it is required that the regularizer parameter is appropriately selected such that the aforementioned problems are avoided.

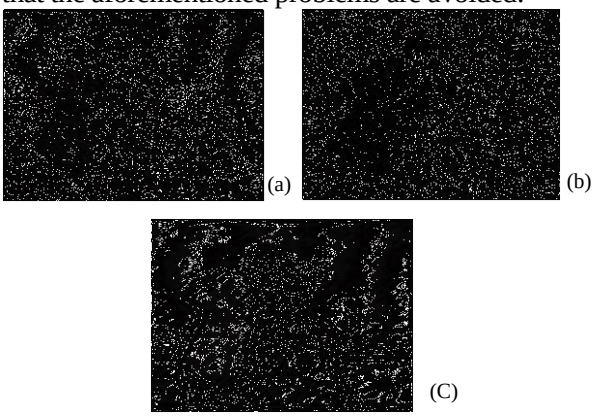

Figure 1. a) Degraded image by 9*9 uniform blur and additive Gaussian noise with zero mean b) restored image by small regularizer parameter ($\tau = 0.001$) c) restored image by large regularizer parameter ($\tau = 10$).

2. Related works

The image restoration methods are classified into three categories: 1) methods bas
ed on filtering 2) methods based on regularizer, and 3) methods based on Bayesian restoration. The image processing systems normally use a low-pass filter to model the blurring of the image. The filter-based methods contain the inverse filtering, pseudo-inverse filtering, and wiener filtering.

Equation (4) results in the restored image using (1) in the Fourier domain [2]:

$$\hat{x} = f^{-1}\left(\frac{Y(\omega_i,\omega_j)}{B(\omega_i,\omega_j)}\right) = f^{-1}\left(X(\omega_i,\omega_j)+\frac{N(\omega_i,\omega_j)}{B(\omega_i,\omega_j)}\right) \quad (4)$$

where, f^{-1} indicates the inverse Fourier transform. $Y(\omega_i,\omega_j)$, $B(\omega_i,\omega_j)$, and $X(\omega_i,\omega_j)$ are 2D Fourier transforms of the degraded image, the blur PSF, and the original image, respectively. The simple theory and low complexity are advantages of the inverse filtering methods. However, the inverse filtering method provides an accurate restoration image when there is not additive noise in the degraded image but the degraded image normally contains an additive noise in practice. Therefore, in a noisy degraded image, the inverse filtering method provides a weak performance and unacceptable results [2].

The pseudo-inverse filtering method uses the matrix-vector form of the degraded image in which B is a non-invertible matrix. If the columns of B are lineally independent, (1) can be modified and approximated using pseudo-inverse solvation as [8]:

$$x = \left(B^T B\right)^{-1} B^T y . \quad (5)$$

The mentioned advantages of inverse filter can be enumerated for the pseudo-inverse filter. This method provides a better performance than the inverse method, although it is unable to provide acceptable results for a noisy degraded image [8].

As the name implies, the median filter is a statistics method. In this method, the median of the pixel is found, and then the pixel is replaced by median of the gray levels in their neighborhood of that pixel. The median filter is used to remove the salt and pepper noise [23].

The Wiener filter method is based upon optimization of Mean Square Error (MSE), and it provides a better performance than the inverse filter. This filter is the base of many new restoration methods because it is an optimal filter to minimize MSE. For example, the edge mapping Wiener filter has been proposed to preserve the edges and the details of images. The collaborative Wiener filter has been reported to remove image noise in a sparse 3D transform domain [9]. Although the Wiener filter is known as the most optimum method for minimization of MSE and can be efficiently solved in frequency domain, it is unable to provide a high quality for the restored image.

The regularization methods were developed to make the image restoration problem well-posed by introducing information about the original image. In this situation, there is a large number of possible solutions; additional information is required to choose the correct solution. Finally, since discontinuities cause instability in many algorithms, the solution must depend continuously upon data. The regularization methods solve this problem using the prior information about the image to calculate the estimate. It requires the selection of a regularization parameter, α, which controls the trade-off between fidelity to measurements and to the prior information.

The regularizer-based method is the second category of the image restoration methods. This method repeatedly combines additional information, and a regularizer solves the restoration problem. These methods, such as Tikhonove-Miller regularizer, are known as a framework to well-pose the restoration problem. The traditional regularizers such as L2-norm adversely affect the sharp edge restoration because the images are piecewise smoothed. Therefore, the advanced regularizers model the characteristics of the original image using non-linear penalty functions [10].

The Bayesian approach provides the means to incorporate prior knowledge in data analysis. The Bayesian analysis revolves around the posterior probability, which summarizes the degree of one's certainty concerning a given situation. The Bayes's law states that the posterior probability is proportional to the product of the likelihood and the prior probability. The likelihood encompasses the information contained in the new data. The prior expresses the degree of certainty concerning the situation before the data is taken. Although the posterior probability completely describes the state of certainty about any possible image, it is often necessary to select a single image as the 'result' or reconstruction. A typical choice is to choose an image that maximizes the posterior probability, which is called the MAP estimate. Other choices for the estimator may be more desirable, for example, the mean of the posterior density function. In situations where only a very limited data is available, the data alone may not be sufficient to specify a unique solution to the problem. The prior introduced with the Bayesian method can help to

guide the result toward a preferred solution. As the MAP solution differs from the maximum likelihood (ML) solution solely because of the prior, choosing the prior is one of the most critical aspects of the Bayesian analysis.

The Bayesian restoration methods model the restoration problem using the probability theory. The Bayesian methods combine additional information of new models of the image with the prior image, and can be iteratively solved. High computational cost and being unable to provide a specific optimization framework are the disadvantages of the Bayesian methods [11].

In this work, we used the regularizer method to restore the image. There are several methods available to solve the linear inverse optimization by minimization of the objective function, which is formulated as:

$$f(x) = \min_x \frac{1}{2}\|y - Bx\|_2^2 + \tau\phi(x) \quad (6)$$

where, B is a linear operator and $\phi(x)$ is a regularizer [4]. This optimization equation should find the best compromise between the candidate estimated, x, and the obtained data of $\|y - Bx\|_2^2$. The undesired degree of equation is distinguished by the $\phi(x)$ parameter, and the relation between two parts of (6) is identified by regulating parameter (τ). The unsmooth and non-quadratic regularizers such as the Total Variant, TV, and l_p -norm are used in various image processing applications [8]. If B = I, where I is a unit vector (identity matrix), the denoising problem is confronted. If $\emptyset$ is suitable and convex, the optimization problem is strictly convex and has a unique minimizer. Therefore, the denoising function is formulated by:

$$\psi_\tau(y) = \arg\min_x \frac{1}{2}\|x - y\|_2^2 + \tau\phi(x) \quad (7)$$

For example, $\psi_\tau(y) = \text{soft}(y, \tau)$ if $\phi(x) = \|x\|_1 = \sum_i |x_i|$ (the L_1norm).

$$\text{soft}(w, \tau) = \text{sign}(w).(|w| - \tau)_+$$

$$\text{where} \quad (a)_+ = \begin{cases} 0 & \text{if } a<0 \\ a & \text{if } a>0 \end{cases}.$$

The soft function is shown in figure 2.

The Iterative Shrinkage Thresholding (IST) methods have been reported to efficiently and simply solve the sparsity-based restoration problems. These methods have firstly been developed as a proximal forward-backward iterative scheme in [12, 13]. In the IST method, x in the k+1 step is obtained by:

$$x^{k+1} = \psi_{\tau/\alpha}\left(x^k - \frac{1}{\alpha_k}\left(B^T\left(Bx^k - y\right)\right)\right) \quad (8)$$

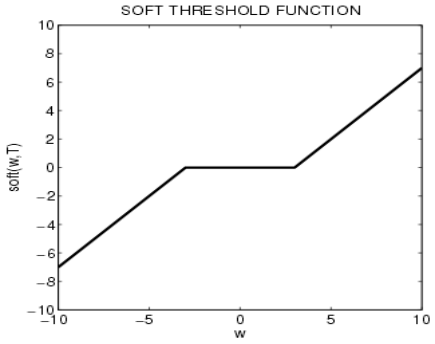

Figure 2. Soft function.

These methods are suitable and efficient when multiplication of B and B^T is dissolvable. These methods converge to minimum when $\|B\|_2^2 / 2 < a_k < +\infty$.

Another method is Two-step Iterative Shrinkage Thresholding (TwoIST), in which each current iterate incorporates to the previous two iterates. The TwoIST method is faster than the IST method. In the TwoIST algorithm, each iteration depends upon the two previous iterates rather than only on the previous one (as in IST). This algorithm may be seen as a non-linear version of the so-called two-step methods for linear problems. TwoIST was shown to be considerably faster than IST on a variety of wavelet-based image restoration problems; the speed gains can reach up to two orders of magnitude in typical benchmark problems [14].

An improved two-step variant of the IST method is called Fast IST Algorithm (FISTA). FISTA is faster than the TwoIST and IST methods. The non-smooth variation of Nesterovs optimal gradient-based algorithm is used in FISTA [15].

Sparse Reconstruction by Separable Approximation Algorithm (SpaRSA) is another fast variant of IST algorithm. This method uses a different α_k in each iteration, which is updated by α_k (where $1/\alpha_k$ is a step size) [12]. This method has been shown to outperform standard IST by selecting an aggressive step-size at each iteration. When the slowness is caused by using a small value of the regularization parameter, the continuation schemes have been found quite effective in speeding up the algorithm. The key observation is that the IST algorithm benefits significantly from warm-starting, i.e. from being initialized near a minimum of the objective function.

Neural Network Approach: The neural network is a form of multi-processor computer system with

simple processing elements interconnected group of nodes [29, 30]. These interconnected components are called neurons, which send message to each other. When an element of the neural network fails, it can continue without any problem by their parallel nature [24].

Block-matching: This is employed to find blocks that contain high correlation because its accuracy is significantly impaired by the presence of noise. We utilize a block-similarity measure that performs a coarse initial denoising in local 2D transform domain. In this method, the image is divided into blocks and noise or blur is removed from each block [23].

Since the reported methods in [25, 26] are based upon non-blind de-convolution and use grayscale images, same databases, and evaluation measures, the proposed method is compared with them. The reported method in [25] is based upon the genetic algorithm, and is briefly given as follows:

Step 1: Get Blurred Image (initial image).

Step 2: Apply Fast Fourier Transform on blurred Image.

Step 3: Apply Inverse Fourier Transform, and create an initial population for applying genetic algorithm .

Step 4: Calculate the value of objective functions for the current population.

Step 5: Apply the cumulative fitness assignment criteria and selection procedure. Use genetic algorithm for selection of new population .

Step 6: Find the best individuals.

Step 7: Apply cross-over and Mutation on the new population (obtained in Step ٥) in order to create a new population .

Step 8: Get the restored image using the best individuals (obtained in Step 6).

This method tries to maximize all the objectives. We proposed a fitness function criterion that is based upon individual objectives such as intensity, entropy, and edges. After evaluating fitness of all individual objectives (entropy, edge, and intensity), the combined fitness or cumulative fitness is calculated. The proposed method evaluates and maximizes all the objectives. This means that the image restoration criterion is defined as a function of entropy, edges, and intensity.

Edges can be defined as rapid changes in image intensity over a small region. In order to measure these changes, one method is to use discrete difference operators. It consists of two masks that calculate the changes in both directions, i.e. x-direction and y-direction.

We took different images with the same size. The maximum number of generation to run the program was chosen as 20; this also works as a criterion to end the evolution. Mutation has to be taken as simple mutation having probability = 0.1, arithmetic cross-over has to be taken having the cross-over probability = 0.8, selection was taken as the tournament selection, and finally, the population size had to be taken as 48.

The reported method in [26] is based upon the Wavelet transform, and is given by:

Step 1: Obtain an initial de-blurred result via the IDD-BM3D method, which will be used as the reference image for support estimation.

Step 2: Solve the resulting truncated ℓ١-regularized problem.

In this work, we just took the anisotropic ℓ1 norm as an example to illustrate the benefit of new regularization, though it can be also readily extended to the isotropic ℓ1 norm.

Ones just solved a plain ℓ1-regularized convex optimization problem, i.e. each frame coefficient was treated equally and penalized uniformly. In this case, it generates the bias, which means that the large coefficients are penalized more heavily than the smaller ones. Therefore, the customized ℓ1-regularized model often achieves a sub-optimal performance. In practice, if the positions of the frame coefficients with large non-zero absolute values (we term the locations of large frame coefficients in magnitudes as support information) are known, we need to remove these coefficients out of the ℓ1 norm and to use a truncated ℓ1 norm instead in the restoration model.

The Gaussian Scale Mixture (GSM) model is developed using the simultaneous sparse coding (SSC), and its applications into image restoration are explored. It is shown that the variances of sparse coefficients (the field of scalar multipliers of Gaussians) can be jointly estimated along with the unknown sparse coefficients via the method of alternating optimization [27].

The so-called non-locally centralized sparse representation (NCSR) model is as simple as the standard sparse representation model, while our extensive experiments on various types of image restoration problems including denoising, deblurring, and super-resolution validate the generality and state-of-the-art performance of the proposed NCSR algorithm.

The patches of image x are clustered into K clusters and a PCA sub-dictionary k is learnt for each cluster. For a given patch, it is firstly checked which cluster it falls into by calculating its distances to means of the clusters, and then the PCA sub-dictionary of this cluster is selected [28].The mentioned methods are unable to converge very fast, and therefore, in this paper, we

propose a new method to increase the speed and also improve the quality of the restored image.

3. Proposed method

We presented a new algorithm to solve the optimization formulation of regularized image restoration. The approach that can be used with different types of regularization is based upon the variable splitting technique. Then it solves the problem with the Lagrangian augmented optimization.

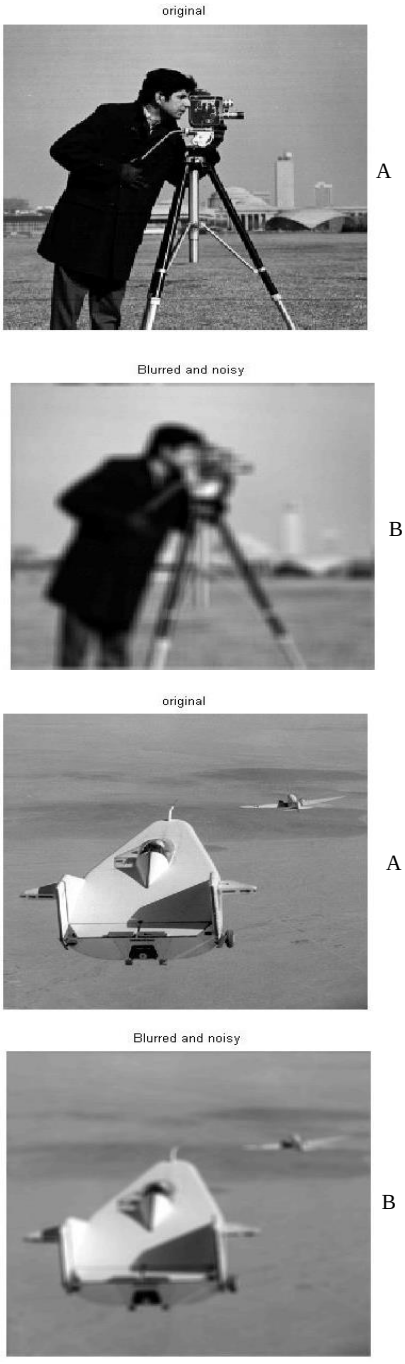

Figure 3. Degraded Cameraman and Lifting-body: A) Original Image and B) degraded image with uniform blur and Gaussian noise.

3.1. Construction of degraded images for deblurring and inpainting

Assume that the aim of the proposed method is to degrade an image with a size of N*N by an m*m uniform blur, where m < N. First, a vector with the length of N is constructed so that the first m elements have the value of 1/m and the rest of the elements are zero. Next, the vector obtained is shifted to left with the size of (m-1)/2, and then it is multiplied by its transpose. Therefore, the m*m matrix is constructed, which is called the blur matrix. In order to obtain the blurred image, it requires to multiply the Fourier transform of the blurred matrix by the Fourier transform of the original image, and then to use inverse Fourier transform. The matrix obtained is Bx indicated in (1). Next, a desired noise is added to Bx, and therefore, the blurred/noisy image is constructed. In order to construct the degraded image for the inpainting case, it requires losing a number of pixels. Losing the pixels is randomly performed. In order to obtain the degraded image in (1), the random matrix is constructed such as a percentage of the original image pixels that is lost.

Note that the size of random matrix is the same as the original image. Some degraded images are shown in figures 3 and 4.

3.2. Solving problem of Lagrangian augmented optimization

In order to obtain the estimated image, x, (2) is used. The proposed method is based upon variable splitting for an optimization problem. The objective function in (2) is the sum of two functions. The main idea in the proposed method is to split the variable of x into the variable pairs of x and v such that each of them is an argument of one part in the objective function. Then the objective function is minimized under one constraint, which results in being equally the new problem with the problem in (2), given by:

$$\min_{x,v\in R^n} \frac{1}{2}\|Bx-y\|_2^2+\tau\phi(v) \quad \text{subject to } x=v \tag{9}$$

The new determined optimization problem is solved by the Lagrangian augmented method. The formulation of undetermined optimization for regulated image restoration is given by:

$$f_1(x)=\frac{1}{2}\|Bx-y\|_2^2 \qquad f_2(x)=\tau\phi(x) \qquad G=I \quad \text{i.e. } v=Gx \tag{10}$$

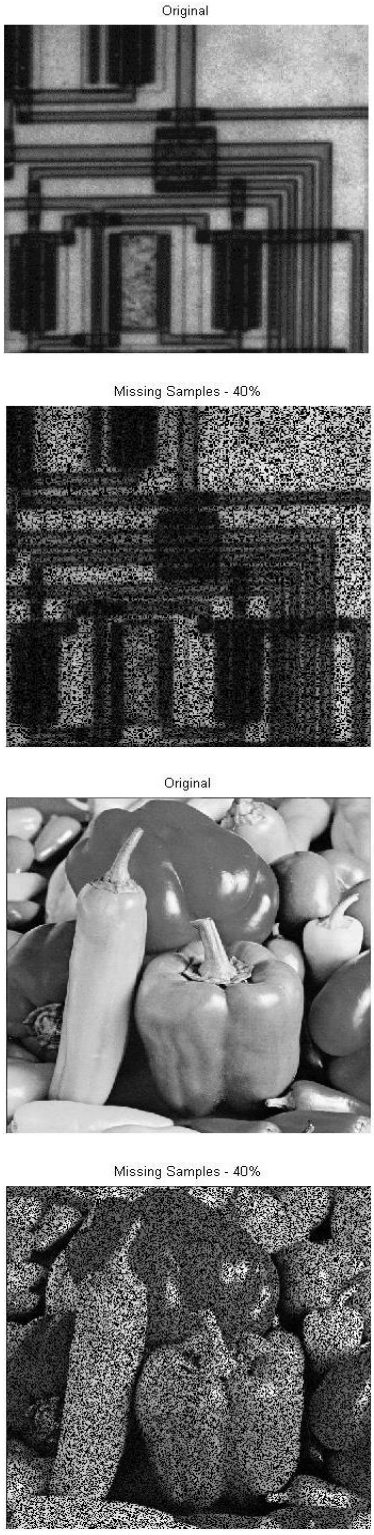

Figure 4. Degraded Cir and Peppers: A) Original Image and B) degraded image with losing 40% of pixels and Gaussian noise.

The formulation of the determined optimization using variable splitting is given by:

$$\text{objective fun} = \min_{x,v\in R^n} \frac{1}{2}\|Bx-y\|_2^2 + \tau\phi(v) \qquad (11)$$

$$\text{subject to } x = v$$

In order to solve the determined optimization problem, it is better to use the Lagrangian augmented method, which is given by:

$$(x_{k+1}, v_{k+1}) \in \arg\min_{x,v} \frac{1}{2}\|Bx-y\|_2^2 + \tau\phi(v) + \frac{\mu}{2}\|x-v-d_k\|_2^2$$
$$d_{k+1} = d_k - (Gx_{k+1} - v_{k+1}) \qquad (12)$$

where, μ is a positive value that is given by the user. It has been shown that the performance of the least-squares penalty is better than the Lagrangian method. In addition, the Lagrangian augmented method is converged under more principle conditions. Therefore, we propose a new method in order to solve the optimization problem, as follows:

First, k is set to zero, and $\mu > 0$, d_0, and v_0 are set to the initial values that are zero, and then it requires to solve the optimization problem given by:

$$x_{k+1} = \arg\min_x \|Bx-y\|_2^2 + \mu\|x-v_k-d_k\|_2^2 \qquad (13)$$

Here, x_{k+1} is a strictly convex function, which has to be minimized. This corresponds to a linear system that is given by:

$$x_{k+1} = \left(B^H B + \mu I\right)^{-1}\left(B^H y + \mu\left(v_k + d_k\right)\right) \qquad (14)$$

By obtaining x_{k+1} from the previous step, it is inserted in (15), and therefore, it requires solving the optimization problem as:

$$v_{k+1} = \arg\min_v \tau\phi(v) + \frac{\mu}{2}\|x_{k+1}-v-d_k\|_2^2 \qquad (15)$$

This can be solved using (7). Then d_{k+1} is obtained by x_{k+1} and v_{k+1} in the previous step:

$$d_{k+1} = d_k - \left(x_{k+1} - v_{k+1}\right) \qquad (16)$$

Next, one is added to k (k = k + 1), and the stop criterion is measured, which is given by:

$$\frac{\left|\text{objective fun}(k+1) - \text{objective fun}(k)\right|}{\left|\text{objective fun}(k)\right|} < \text{tolerance} \qquad (17)$$

This criterion is equal to the changes of the objective function. If the stop criterion is satisfied, the procedure is stopped; otherwise the previous steps are repeated until the stop criterion is satisfied.

3.2.1. Variable splitting: Consider the undetermined optimization problem, which contains two terms:

$$\min_{x\in R^n} f_1(x) + f_2(g(x)), \qquad (18)$$

where, the $g: R^n \to R^d$ variable splitting includes construction of a new variable as $g(x) = v$ that corresponds to a new optimization problem, given by:

$$\min_{x \in \square^n, v \in R^d} f_1(x) + f_2(v) \quad s.t: g(x) = v \tag{19}$$

This is equal to the optimization problem in (18). We use the variable splitting method reported in [7] to provide a fast restoration image. In [4, 10], the optimization problem in (19) is changed to (20) with consideration of the second order penalty and the periodical minimization with respect to x and v.

$$\min_{x \in R^n, v \in \square^d} f_1(x) + f_2(v) + \frac{\alpha}{2}\|g(x) - v\|_2^2 \tag{20}$$

The function of variable splitting is as the one reported by Bregman [18, 19]. This directly solves the determined optimization problem. It has been shown that when g is a linear function, i.e. $g(x) = Gx$, the Bregman′s method is similar to the Lagrangian augmented method.

3.2.2. Lagrangian augmented: Consider the optimization problem with constraint as follows:

$$\min_{z \in R^n} E(z) \quad s.t\ Hz - b = 0 \tag{21}$$

where, b = 0, $z = \begin{bmatrix} X \\ V \end{bmatrix}$ and $H = [G \quad -I]$.

In this case, the Lagrangian function is given by:

$$L_A(z, \lambda, \mu) = E(z) + \lambda^T(b - Hz) + \frac{\mu}{2}\|Hz - b\|_2^2 \tag{22}$$

where, λ is a value for the Lagrangian coefficient, and $\mu > 0$ is called the penalty parameter. In this method, $L_A(z, \lambda, \mu)$ is minimized with respect to z and maintaining λ as a constant value, and then λ is updated and the minimization of $L_A(z, \lambda, \mu)$ is repeated. This procedure continues until the convergence criterion is satisfied [20].

3.2.3. Variable splitting using Lagrangian augmented method: Consider the variable splitting problem given by:

$$\min\ R(x) + \tau\phi(v) \quad s.t \quad v = Gx. \tag{23}$$

where, R(.) is the fidelity term that guarantees that x is compatible with the observed y.
In this case, the Lagrangian augmented method is given by:

$$L_\rho(x, v, \mu) = R(x) + \tau\phi(v) + \mu^T(Gx - v) + \frac{\rho}{2}\|V - Gx\|_2^2 \tag{24}$$

where, μ is the Lagrangian coefficients vector and is a constant that is selected by a user [21]. We use the Gauss–Seidel method for minimization. Therefore, the minimization problem is formulated as:

$$x_{k+1} = \arg\min_x L_\rho(x_k, v_k, \mu_k), \tag{25}$$

$$v_{k+1} = \arg\min_v L_\rho(x_{k+1}, v_k, \mu_k), \tag{26}$$

$$\mu_{k+1} = \mu_k + \rho(Gx_{k+1} - v_{k+1}). \tag{27}$$

3.2.4. Total variation regularizer: Total variation regularizers, due to having the ability for noise cancellation and maintaining image edges, are widely used in the image restoration methods [7]. These regularizers have improved under this assumption that the image has bounded variations. If the variations of the image inside are bounded, then the sum of the absolute variations of the image inside will be limited.
Therefore, the total variation regularizers are designed to restrict the variations of the image inside. The variation is defined by:

$$\phi(x) = \sum_{w=1}^{l} \sqrt{\nabla_i(x_w)^2 + \nabla_j(x_w)^2}, \tag{28}$$

where, $\nabla_i(x_w)$ and $\nabla_j(x_w)$ are the first-order vertical and horizontal difference in the i^{th} pixel, respectively. On the other hand, the sparsity regularizer causes the transform coefficients of the restored images to be scattered. These regularizers reduce the noise without any destructive effect on the edges.

3.2.5. Calculation of x_{k+1}: In (14), the initial vales for x_0, d_0, and v_0 are set to zero. Thus in (28), $\phi(v_0)$ that is related to the total variation regularizer can be solved and $\|Bx_0 - y\|_2^2$ can be calculated using (3). The initial objective function is then calculated using $\phi(v_0)$ and $\|Bx_0 - y\|_2^2$. In what follows, calculation of x_{k+1} is distinctly explained for the deblurring/denoising and inpainting problems.

A) Calculation of x_{k+1} for deblurring/denoising: First, the absolute of Fourier transform of blur matrix, B, is obtained and each element is squared and added with μ:

$$(B^{H}B+\mu I)^{-1}, \quad (29)$$

The matrix elements obtained are then inversed. Next, the Fourier transform of $B^{H}y+\mu(v_k+d_k)$ is obtained and multiplied by (20). x_{k+1} is the inverse Fourier transform of the resulting matrix.

B) Calculation of x_{k+1} for inpainting: In order to obtain the inverse of $(B^{H}B+\mu I)$, the Sherman-Morrison-Woodbury equation is used, which is given by:

$$\left(B^{H}B+\mu I\right)^{-1}=\frac{1}{\mu}\left(I-\frac{1}{\mu+1}B^{H}B\right), \quad (30)$$

where, $B^{H}B$ is a number of zeros in the main diagonal. These zeros indicate the lost positions in the image.

Thus x_{k+1} is obtained by multiplication of $B^{H}y+\mu(v_k+d_k)$ with (30).

3.2.6. Calculation of v_{k+1}: v_{k+1} can be calculated by the Moreau proximal mapping for $x_{k+1}-d_k$. This means that:

$$v_{k+1}=\psi(x_{k+1}-d_k), \quad (31)$$

where, ψ is given by equation (9). If this mapping is accurately calculated in the closed form, then it is guaranteed that the proposed method is converged.

4. Results

All experiments were executed using the MATLAB software, applied on a personal computer containing a microprocessor of Intel (R) i5CPU:2.53 GHz and 4 GB RAM. The value for μ in (13) was selected as 10% of the regularizer parameter or $\tau/10$.

The number of iterations, the processing time (CPU time), ISNR, and MSE were used as the evaluation measures. We used various images such as cameraman, Lena, moon, lifting-body, tire, coins, and peppers. For blurring, we used a uniform blur with a size of 9*9 and white normal Gaussian noise with different variances, and for inpainting, 30%, 40%, and 50% of the original pixels were lost.

4.1. Evaluation measures

In order to compare the performance of the different image restoration methods, the quantitative measures that evaluate the quality of the restored image are very important. These measures include Improvement in SNR, ISNR, and Mean Square Error (MSE), which are calculated by [2, 9]:

$$\mathrm{ISNR}=10\log_{10}\frac{\sum_K\|x-y_k\|^2}{\sum_K\|x-\hat{x}_k\|^2} \quad (32)$$

$$\mathrm{MSE}=\frac{1}{M*N}\sum_K\|x-\hat{x}_k\|^2 \quad (33)$$

where, M and N are the image dimensions, x is the original image, and y_k and $\hat{x}_k$ are the observed and the estimated image in the k^{th} iteration. In this work, in addition to these two measures, the processing time was also considered, which indicates the speed of convergence for capability of the methods.

4.2. Indexing results

4.2.1. Results obtained for deblurring

Table 1 shows the evaluation measures for the aforementioned images. The results obtained show that the proposed method improves ISNR, decreases MSE, and reduces the processing time considerably compared to the TwoIST and SpaRSA methods.

Table 1. Results of deblurring images degraded by Gaussian noise with $\sigma = 0.3080$ and Uniform blur 9*9 in size.

Image	Method	Iterations	CPU time (s)	ISNR (dB)	MSE
Cameraman	TwoIST	69	16.2	7.63	94.1
	SpaRSA	123	25.7	7.86	89.2
	Proposed method	20	3.67	8.43	78.2
Lena	TwoIST	46	51.1	6.56	37.4
	SpaRSA	56	52	6.36	39.1
	Proposed method	16	13.1	7.59	29.5
Lifting-body	TwoIST	41	45.3	8.64	12.3
	SpaRSA	53	49.5	8.88	11.6
	Proposed method	24	20.3	10.4	8.14
Coins	TwoIST	61	13.8	8.87	54.4
	SpaRSA	115	23.1	8.71	56.5
	Proposed method	22	4.06	9.75	44.5
Moon	TwoIST	25	13.1	3.86	62.8
	SpaRSA	22	9.14	3.73	70.2
	Proposed method	17	6.18	3.91	67.4
Peppers	TwoIST	51	55.5	7.93	31.8
	SpaRSA	78	73.4	7.97	30.1
	Proposed method	18	14.8	8.45	27

As observed in table 1, for instance, for the Lena image, ISNR was improved by the proposed method 1.03 dB and 1.23 dB compared to the TwoIST and SpaRSA methods, respectively, and

the processing time was nearly 25% of the one provided by the TwoIST and SpaRSA methods. In addition, MSE obtained by the proposed method decreased 10 units. For the Lifting-body image, the processing time required by the proposed method was less than half of the ones resulted by the other two methods and ISNR improved around 1.5 dB. In addition, MSE decreased to 3.46 and 4.16 compared to the SpaRSA and TwoIST methods, respectively.

Figure 5 shows the objective function indicated in (8) for the aforementioned images. As observed, the objective function compared to the SpaRSA and TwoIST methods is faster converged. For instance, for the cameraman image, the objective function is converged to the final value in less than 4 s, whereas 30 s is required for the other two methods at least. For the Lena image, the proposed method is converged in 3 s, whereas the SpaRSA and TwoIST methods require 30 s and 50 s, respectively, for convergence. The same results can be observed for the other images. As an example, figures 6-9 show the restored image by the proposed method. As observed, the blurred effect has been highly removed in the restored image by the proposed method.

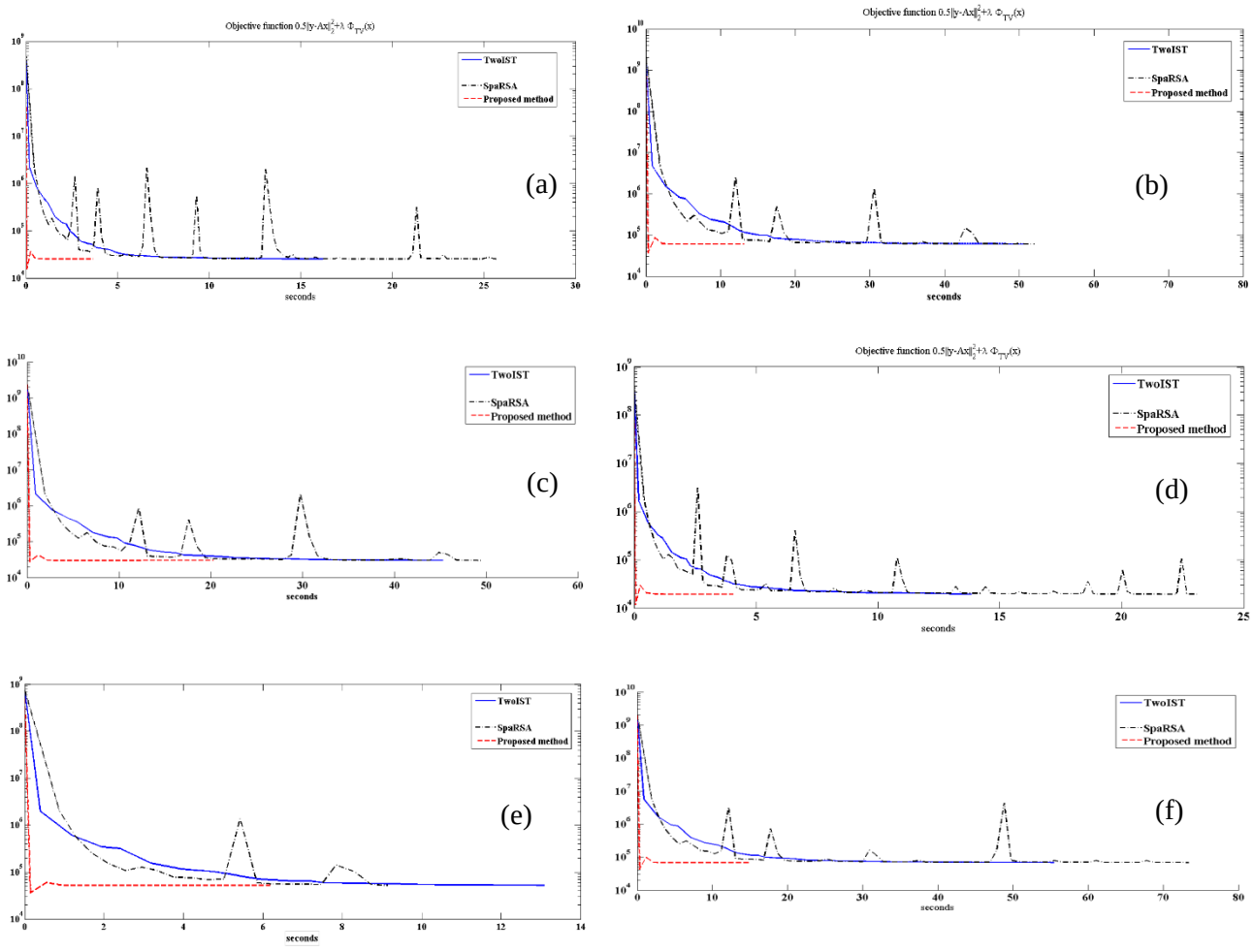

Figure 5. Output of deblurring for objective function related to equation (8) obtained by TwoIST, SpaRSA, and proposed method for images: A) Cameraman, B) Lena, C) Lifting-body, D) Coins, E) Moon, and F) Peppers.

Figure 6. Deblurring results: A) Original Image, B) degraded image, and C) restored image by proposed method.

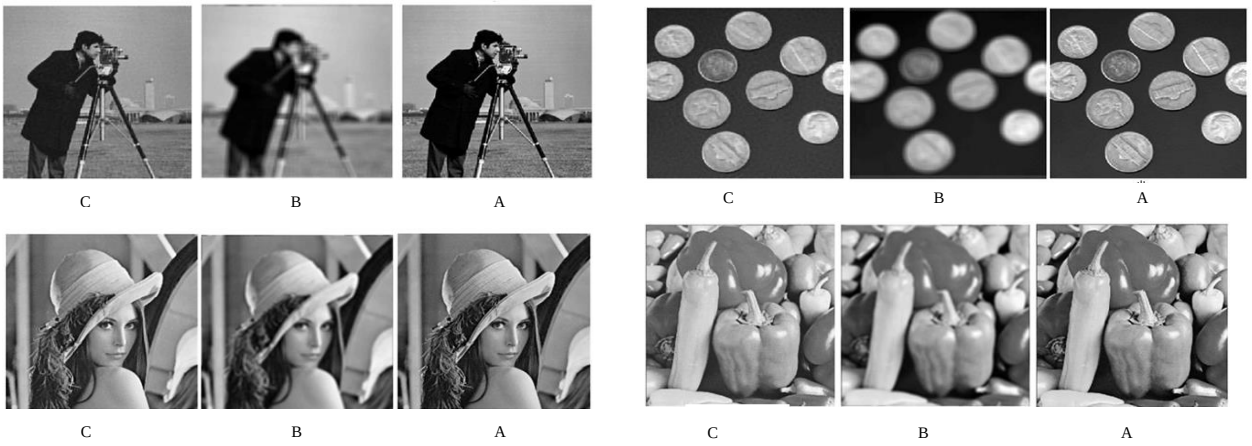

Figure 7. Deblurring results for Cameraman, Coins, Lena, and Peppers: A) Original Image, B) degraded image, and C) restored image by proposed method.

In the next experiment, the effect of different blurs with additive Gaussian noise ($\sigma = 0.3080$) was investigated. The results obtained are shown in table 2. As observed, the processing time (CPU time), ISNR, and MSE were improved compared to the other methods. It was also observed that the best results with respect to ISNR and MSE were achieved by uniform blur with a size of 9*9. In addition, the results obtained for the case of Gaussian blur with $\sigma = 1.41$ were better than the one with $\sigma = 2.83$. In the case of blur matrix in which $h_{i,j}=1/(1+i^2+j^2)$ for i,j=-7,...7 , the results obtained provided higher ISNR and lower MSE and CPU time compared to the other cases.

In another experiment, the effect of different additive noises with uniform blur with a size of 9*9 was examined. As expected, the results obtained show that when the variance of Gaussian noise increases, ISNR decreases, MSE increases, and the quality of the restored image degrades. As an example, tables 3-7 show the results obtained for different images using different blurs and Gaussian noise with $\sigma = 0.3080$, $\sigma = 0.5$, and $\sigma = 2.0$.

In tables 5 and 7, the values for Peak Signal for the restored images by the proposed method and other methods are shown. The PSNR values by the proposed method are higher than the results obtained by the TwoIST, SpaRSA, Genetic Algorithm, Wavelet Frame Truncated, NCSR, and SSC-GSM methods. As shown, the results obtained by the proposed method are better in terms of the Peak Signal to Noise Ratio.

In tables 5 and 6, the MSE values for the restored images by different images are shown. The MSE values by the proposed method are less than the results obtained by the TwoIST, SpaRSA, Genetic Algorithm, Wavelet Frame Truncated, NCSR, and SSC-GSM methods.

Similar results were obtained for the other images, which seem to be unnecessary to be shown.

4.2.2. Results obtained for inpainting

In the inpainting problem, the aim is the restoration of the degraded image in which a percentage of the pixels has been lost and noise has been added. In this experiment, 40% of the image pixels were lost and a normal white Gaussian noise was added to the image. For evaluation, the aforementioned images were used and the proposed method was compared to the TwoIST and FISTA methods. The results

obtained were shown in table 8. As observed, the proposed method resulted in a higher ISNR, a lower MSE, and also a shorter processing time compared to the TwoIST and FISTA methods. For instance, for the Lena image, the processing time was almost 10% of the one provided by the other two methods and improved ISNR and MSE at least 0.3 dB and 1.2, respectively. For the lifting-body image, the processing time was around 1000 s and 845 s less the ones obtained for the TwoIST and FISTA methods, respectively. Also ISNR obtained by the proposed method was 0.64 dB and 0.97 dB higher than the ones resulted by the TwoIST and FISTA methods, respectively. In this case, the proposed method provided 0.4 and 0.5 reduction in MSE compared to the FISTA and TwoIST methods, respectively. The same results could also be concluded for other images.

Figure 10 shows the objective function resulted by inpainting for the aforementioned images. As observed, the resulting objective function by the proposed method can converge to the final value in a shorter time compared to the TwoIST and FISTA methods. For instance, in figure 10(a), which is related to the cameraman image, the objective function converges in 50 s, 200 s, and 300 s for the proposed method, TwoIST, and the FISTA method, respectively. The same results can be observed for the other images. Therefore, the objective function by the proposed method converges faster than the other two methods.

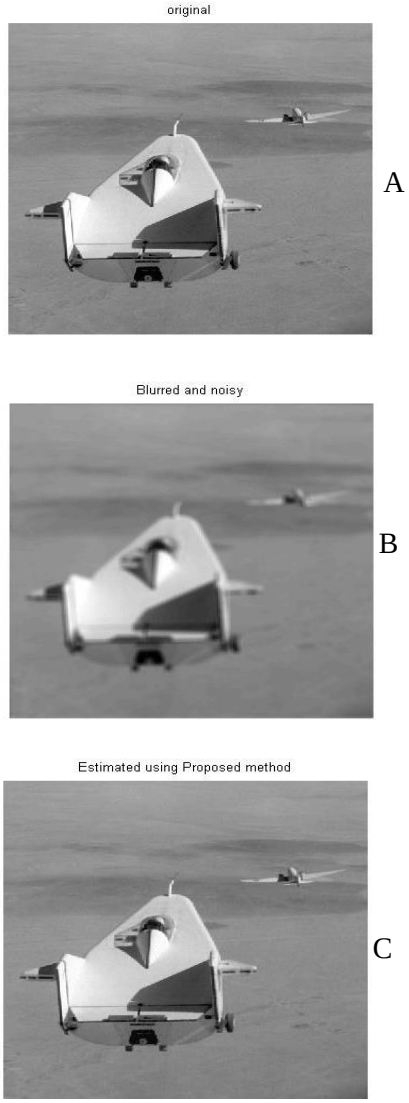

Figure 8. Deblurring results for Lifting-body: A) Original Image, B) degraded image, and C) restored image by proposed method.

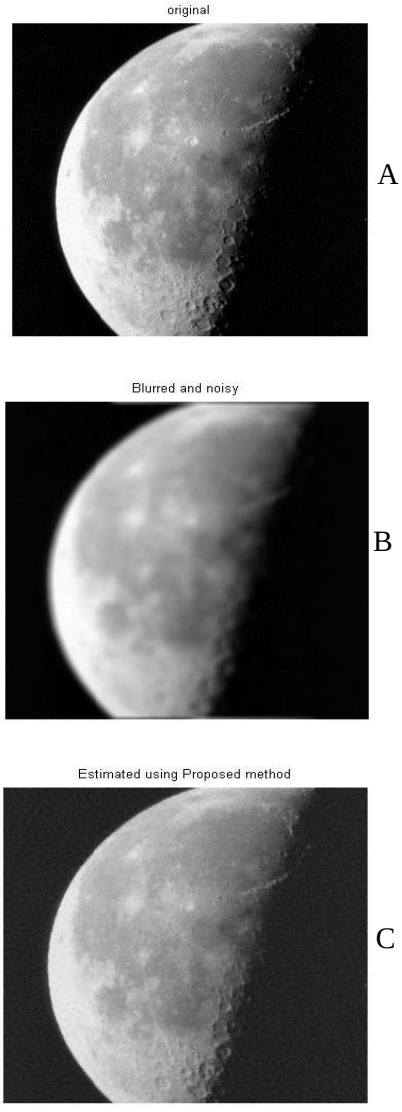

Figure 9. Deblurring results for Moon: A) Original Image, B) degraded image, and C) restored image by proposed method.

Table 2. Results of restored images degraded by Gaussian noise with $\sigma = 0.3080$ and different blurs.

Image	Method	Uniform blur with size of 9*9			Gaussian blur with $\sigma = 1.41$		
		CPU time(s)	ISNR (dB)	MSE	CPU time(s)	ISNR (dB)	MSE
Cameraman	TwoIST	62.45	5.24	94،1	26.59	3.65	113.27
	SpaRSA	64.5	5.92	89،1	22.73	3.71	107.78
	Proposed method	11.01	8،43	78،2	1.45	4.19	92.76
Lena	TwoIST	51،1	6،56	37،4	25.4	2.87	99.1
	SpaRSA	52	6،36	39،1	26.7	2.34	63.7
	Proposed method	13،1	7،59	29،5	3.9	3.42	49.8
Lifting-body	TwoIST	45،3	8،64	12،3	19.9	4.52	34.1
	SpaRSA	49،5	8،88	11،6	21.4	4.69	28.9
	Proposed method	20،3	10،4	8،14	11.9	5.73	22.7
Coins	TwoIST	13،8	8،87	54،4	16.2	4.95	67.7
	SpaRSA	23،1	8،71	56،5	29.5	4.99	65.4
	Proposed method	4،06	9،75	44،5	1.36	5.74	50.2
Moon	TwoIST	13،1	3،86	68،2	17.7	1.27	79.4
	SpaRSA	9،14	3،73	70،2	24.01	1.31	90.7
	Proposed method	6،18	3،91	67،4	1.47	2.07	70.9
Peppers	TwoIST	55،5	7،73	31،8	29.78	3.75	44.8
	SpaRSA	73،4	7،97	30،1	36.6	3.81	42.9
	Proposed method	14،8	8،45	27	4.39	4.49	37.7
		Gaussian blur with $\sigma = 2.83$			Blur matrix $h_{i,j}=1/(1+i^2+j^2)$ for i,j=-7,...7		
		CPU time(s)	ISNR (dB)	MSE	CPU time(s)	ISNR (dB)	MSE
Cameraman	TwoIST	24.21	2.57	79.7	19.25	4.64	100.6
	SpaRSA	23.18	2.69	69.8	17.45	4.61	98.2
	Proposed method	2.67	3.35	58.98	1.41	6.05	81.3
Lena	TwoIST	23.64	1.36	110	19.47	3.45	45.3
	SpaRSA	25.01	1.70	75	24.88	3.49	43.7
	Proposed method	4.12	3.29	50.45	3.25	6.21	35.4
Lifting-body	TwoIST	15.89	3.44	59.2	14.35	5.41	38.3
	SpaRSA	19.46	3.55	54.3	15.18	5.56	32.1
	Proposed method	12.10	5.41	43.9	9.42	8.35	21.6
Coins	TwoIST	14.75	3.81	79.1	13.89	4.99	60.7
	SpaRSA	23.40	3.86	63.7	22.70	5.01	62.9
	Proposed method	2.41	5.24	46.7	1.32	8.31	55.4
Moon	TwoIST	15.14	0.904	95.1	12.36	2.35	71.3
	SpaRSA	18.95	0.915	91.35	16.87	2.47	84.7
	Proposed method	2.56	1.86	79.4	1.48	4.95	61.6
Peppers	TwoIST	21.27	2.62	76	21.12	4.26	39.4
	SpaRSA	30.49	2.76	75.2	28.64	4.95	40.8
	Proposed method	5.17	4.24	60.9	3.39	7.12	30.7

Table 3. Results of restored cameraman image degraded by uniform blur with size of 9*9 and different noises.

Method	MSE				ISNR			
	Poisson noise	Gaussian noise with variance 2	Gaussian noise with variance 1	Gaussian noise with variance 0.308033	Poisson noise	Gaussian noise with variance 2	Gaussian noise with variance 1	Gaussian noise with variance 0.308033
TwoIST	$1.07' 10^4$	166	148	94،1	–10.6	5.17	5.21	7.63
SpaRSA	2.86×10^3	141	138	89،1	–4.83	5.87	5.95	7.86
Wiener filter	1.11×10^4	8.93×10^3	8.93×10^3	8.93×10^3	–10.7	0.629	0.633	1.28
Inverse filter	1.06×10^9	2.5×10^6	5.5×10^5	2.4×10^5	–60.5	–35.8	–30	–14.6
Proposed method	1.99×10^3	134	132	78،2	–3.27	6.08	6.14	8.43

Table 4. Results of restored Lena image degraded by uniform blur with size of 9*9 and different noises.

Method	MSE				ISNR			
	Poisson noise	Gaussian noise with variance 2	Gaussian noise with variance 1	Gaussian noise with variance 0.308033	Poisson noise	Gaussian noise with variance 2	Gaussian noise with variance 1	Gaussian noise with variance 0.308033
TwoIST	7.14×10^3	101	100	37،4	–10.6	5.42	5.45	6،56
SpaRSA	1.79×10^3	100	99.6	39،1	–4.83	5.45	5.48	6،36
Wiener filter	9.41×10^3	3.94×10^3	3.94×10^3	3.94×10^3	–10.7	0.435	0.438	0.891
Inverse filter	4.47×10^8	1.22×10^6	7.23×10^5	4.91×10^4	–60.5	–35.4	–30.31	–15.01
Proposed method	1.27×10^3	95	80.2	29،5	–3.27	5.92	6.08	7،59

Table 5. Results of MSE and PSNR restored images degraded by Gaussian noise with σ = 2 and different blurs.

Image	Blur	TwoIST	SpaRSA	Genetic Algorithm	Wavelet Frame Truncated	NCSR	SSC-GSM	Proposed method
				PSNR				
Cameraman	9 × 9 uniform blur	25.45	25.97	27.94	27.97	28.62	28.82	28.89
	Gaussian blur: (σ =1.6)	26.27	26.35	27.48	27.78	28.33	28.39	28.53
	Motion blur: fspecial (‘motion’, 15, 30)	27.78	27.87	29.54	29.77	29.80	29.86	29.93
Lena	9 × 9 uniform blur	27.09	27.63	29	29.04	29.87	29.94	30.10
	Gaussian blur: (σ =1.6)	26.62	26.76	30.87	30.93	30.90	31.04	31.29
	Motion blur: fspecial (‘motion’, 15, 30)	28.81	28.91	31.17	31.20	31.41	31.79	32.91
				MSE				
Cameraman	9 × 9 uniform blur	185.39	164.468	104.49	103.77	89.35	85.33	83.96
	Gaussian blur: (σ = 1.6)	153.49	150.68	116.16	108.41	95.52	94.21	91.21
	Motion blur: fspecial (‘motion’, 15, 30)	110.17	106.19	72.30	68.56	68.09	67.15	66.08
Lena	9 × 9 uniform blur	129.74	112.22	81.86	81.1	67.00	65.93	66.84
	Gaussian blur: (σ =1.6)	141.60	137.1	53.22	52.49	52.85	51.19	48.31
	Motion blur: fspecial (‘motion’,15,30)	86.12	83.57	49.67	49.33	46.99	43.06	33.27

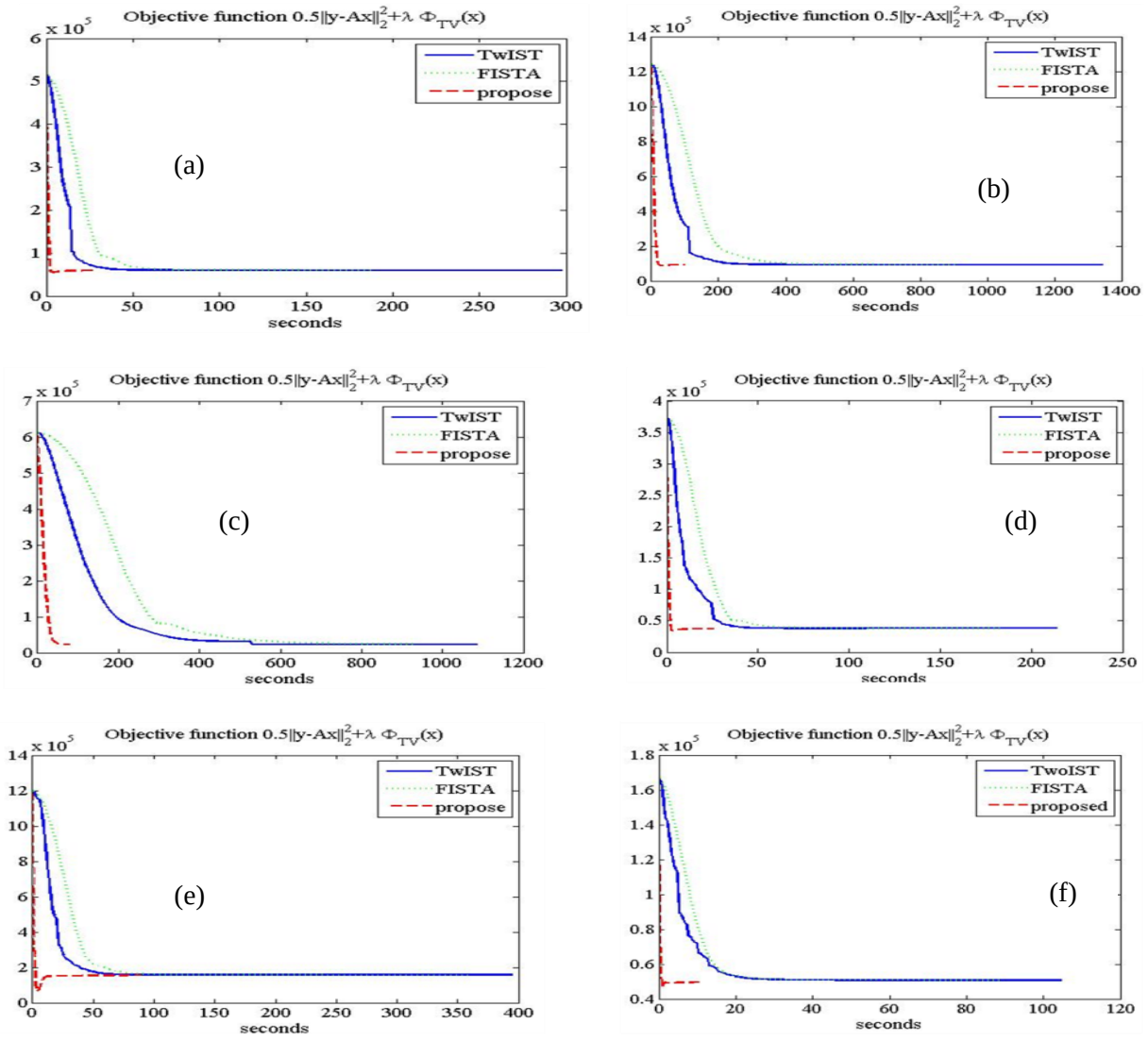

Figure 10. Output of inpainting for objective function related to equation (8) obtained by TwoIST, FISTA, and proposed methods for images: A) Cameraman, B) Lena, C) Lifting-body, D) Coins, E) Moon, F)Tire, and G) Peppers.

Table 6. Results of MSE restored images degraded by Gaussian noise with $\sigma = 0.5$ and different blurs.

image	Cameraman	Lena	Butterfly	Foreman	House	Leaves	moon	baboon	Barbara	Peppers
9 × 9 uniform blur, σ = 0.5										
TwoIST	100.71	48.32	89.94	32.89	27.73	86.51	84.74	306.96	99.10	42.18
SpaRSA	96.40	43.56	87.04	31.99	26.55	81.86	82.05	305.25	94.86	41.50
Genetic Algorithm	65.48	41.50	61.46	25.83	18.15	75.70	77.10	272.95	77.28	39.27
Wavelet Frame Truncated	64.58	42.27	59.13	22.97	18.36	75.00	76.75	275.47	76.93	40.18
NCSR	64.72	41.69	52.13	22.14	18.48	65.17	78.00	248.50	81.67	41.31
SSC-GSM	63.39	41.41	51.66	22.03	18.01	52.37	74.83	266.73	79.26	41.12
Proposed method	52.49	32.33	50.38	15.00	10.59	43.65	69.51	224.95	53.10	31.75
Gaussian blur: (σ =1.6), Gaussian noise with σ = 0.5										
TwoIST	87.92	110.05	74.99	39.09	27.87	61.96	87.52	327.40	105.70	66.85
SpaRSA	85.92	68.53	67.91	38.46	26.42	60.82	98.42	325.15	101.41	66.37
Genetic Algorithm	82.24	56.03	49.14	33.27	25.30	55.60	88.73	300.66	83.96	59.30
Wavelet Frame Truncated	81.68	53.78	50.86	26.48	23.34	54.46	92.27	293.14	85.52	58.89
NCSR	82.61	51.77	52.25	26.98	21.63	46.46	96.18	299.97	95.08	59.99
SSC-GSM	81.67	49.90	48.87	21.88	20.28	39.54	94.21	302.75	86.91	57.29
Proposed method	61.96	45.32	46.35	19.81	13.55	38.73	74.83	242.70	77.64	41.79
Motion blur: fspecial ('motion', 20, 45), σ = 0.5										
TwoIST	87.51	51.40	73.69	65.62	32.14	76.22	81.67	318.48	92.70	43.16
SpaRSA	85.92	49.78	69.87	30.34	30.34	71.96	77.28	325.15	87.72	41.22
Genetic Algorithm	76.75	39.86	53.76	22.28	21.29	59.44	71.13	263.08	75.52	44.47
Wavelet Frame Truncated	75.35	39.54	52.41	21.38	20.66	58.89	68.72	260.66	79.13	34.84
NCSR	79.63	36.99	52.73	22.70	21.09	51.53	71.13	266.73	72.29	36.23
SSC-GSM	75.52	34.28	51.53	20.61	20.00	46.57	67.46	260.06	78.40	34.84
Proposed method	52.73	30.21	30.18	11.54	11.78	25.89	62.24	227.03	51.77	24.84

Table 7. Results of PSNR restored images degraded by Gaussian noise with $\sigma = 0.5$ and different blurs.

image	Cameraman	Lena	Butterfly	Foreman	House	Leaves	moon	baboon	Barbara	Peppers
9 × 9 uniform blur, σ = 0.5										
TwoIST	28.10	31.38	28.59	32.96	33.70	28.76	28.85	23.26	28.17	31.88
SpaRSA	28.29	31.74	28.73	33.08	33.89	29.00	28.99	23.27	28.36	31.95
Genetic Algorithm	29.97	31.95	30.25	34.01	35.54	29.34	29.26	23.77	29.25	32.19
Wavelet Frame Truncated	30.03	31.87	30.41	34.52	35.49	29.38	29.28	23.73	29.27	32.09
NCSR	30.02	31.93	30.96	34.68	35.48	29.99	29.21	23.59	29.01	31.97
SSC-GSM	30.11	31.96	30.999	34.70	35.59	30.94	29.39	23.87	29.14	31.99
Proposed method	30.93	33.05	31.11	36.37	37.88	31.73	29.71	24.61	30.88	33.11
Gaussian blur: (σ = 1.6), Gaussian noise with σ = 0.5										
TwoIST	28.69	27.71	29.38	32.21	33.68	30.21	28.71	22.98	27.89	29.88
SpaRSA	28.79	29.77	29.81	32.28	33.91	30.29	28.29	23.01	28.07	29.91
Genetic Algorithm	28.98	30.65	31.22	32.91	34.10	30.68	28.65	23.35	28.89	30.40
Wavelet Frame Truncated	29.01	30.82	31.07	33.90	34.45	30.77	28.48	23.46	28.81	30.43
NCSR	28.96	30.99	30.95	33.82	34.78	31.46	28.30	23.36	28.35	30.35
SSC-GSM	29..01	31.15	31.24	34.73	35.06	32.16	28.39	23.32	28.74	30.56
Proposed method	30.21	31.57	31.47	35.16	36.81	32.25	29.39	24.28	29.23	31.92
Motion blur: fspecial ('motion', 20, 45), σ = 0.5										
TwoIST	28.71	31.02	29.47	29.96	33.06	29.31	29.01	23.10	28.46	31.78
SpaRSA	28.79	31.16	29.68	33.31	33.31	29.56	29.25	23.01	28.70	31.98
Genetic Algorithm	29.28	32.13	30.83	34.65	34.85	30.39	29.61	23.93	29.35	32.65
Wavelet Frame Truncated	29.36	32.16	30.94	34.83	34.98	30.43	29.76	23.97	29.49	32.71
NCSR	29.12	32.45	30.91	34.57	34.89	31.01	29.61	23.82	29.54	32.54
SSC-GSM	29.35	32.78	31.01	34.99	35.12	31.45	29.84	23.99	29.78	32.71
Proposed method	30.91	33.33	33.34	37.51	37.42	34.00	30.19	24.57	30.99	34.18

As an example for inpainting, figures 11-14 show the restored image by the proposed method. As observed, the restored image is highly similar to the original one.

In the next experiment, the effect of different percentages of losing pixels with additive Gaussian noise with $\sigma = 0.308033$ and $\sigma = 1.0$ was investigated. As expected, as the percentage of losing the pixels increases, ISNR decreases, and MSE and CPU time increases. As an example, tables 9-11 show the results obtained for the Cameraman, Lena, and Lifting-body images, respectively. The same results were obtained for the other images, which seem to be unnecessary to be presented.

A B C

Figure 11. Results of inpainting: A) Original Image, B) degraded image, and C) restored image by proposed method.

Table 8. Results of inpainting images degraded by Gaussian noise with $\sigma = 0.3080$ and Losing 40% of pixels.

Image	Method	Iterations	CPU time(s)	ISNR (dB)	MSE
Cameraman	TwoIST	502	313	18.8	95.6
	SpaRSA	500	194	19	90.7
	Proposed method	73	27.5	19.2	85.7
Lena	TwoIST	502	1340	24.9	22.7
	SpaRSA	500	915	25.2	21
	Proposed method	55	100	25.5	19.8
Lifting-body	TwoIST	502	1080	7.96	30.2
	SpaRSA	500	925	7.64	30.3
	Proposed method	44	79.7	8.61	29.8
Coins	TwoIST	502	214	17.4	112
	SpaRSA	500	184	18.1	95.6
	Proposed method	78	25.9	18.3	90.9
Moon	TwoIST	502	1059	21.7	37
	SpaRSA	500	1499	21.9	35.3
	Proposed method	127	256	23.1	33.5
Tire	TwoIST	502	105	15.3	85.1
	SpaRSA	500	89	16	71.5
	Proposed method	63	11.3	16.7	61.9
Peppers	TwoIST	502	803	24.1	26.3
	SpaRSA	500	559	24.3	25.7
	Proposed method	61	72.6	24.9	22.6
Cir	TwoIST	502	294	19.3	36.8
	SpaRSA	500	204	19.4	36.2
	Proposed method	6.57	6.57	19.5	35.4

Table 9. Results of inpainting for cameraman image with different degradations.

	Method	Losing 30% of pixels			Losing 40% of pixels			Losing 50% of pixels		
		CPU time(s)	ISNR (dB)	MSE	CPU time(s)	ISNR (dB)	MSE	CPU time(s)	ISNR (dB)	MSE
Gaussian noise with variance 0.308033	TwoIST	374	66.5	19.2	313	95.6	18.8	404	144	17.9
	FISTA	274	62.7	19.5	194	90.7	19	274	135	18.2
	Proposed method	22.3	60.7	22.7	27.5	85.7	19.2	33.6	129	18.4
	Method	**Losing 30% of pixels**			**Losing 40% of pixels**			**Losing 50% of pixels**		
		CPU time(s)	**ISNR (dB)**	**MSE**	**CPU time(s)**	**ISNR (dB)**	**MSE**	**CPU time(s)**	**ISNR (dB)**	**MSE**
Gaussian noise with variance 1	TwoIST	315	68	19	476	101	18.5	532	143	18
	FISTA	291	64	19.3	274	93.2	18.6	288	139	18.1
	Proposed method	38.6	48.8	20.5	39.4	80.4	19.1	39.5	114	18.3

Table 10. Results of inpainting for Lena image with different degradations.

	Method	Losing 30% of pixels			Losing 40% of pixels			Losing 50% of pixels		
		CPU time(s)	ISNR (dB)	MSE	CPU time(s)	ISNR (dB)	MSE	CPU time(s)	ISNR (dB)	MSE
Gaussian noise with variance 0.308033	TwoIST	134	61.3	19.3	273	93	18.8	158	122	18.5
	FISTA	115	60.8	19.3	175	89	19	119	115	18.6
	Proposed method	10.2	59.2	19.4	10.9	85.7	19.2	11	113	18.7
	Method	**Losing 30% of pixels**			**Losing 40% of pixels**			**Losing 50% of pixels**		
		CPU time(s)	**ISNR (dB)**	**MSE**	**CPU time(s)**	**ISNR (dB)**	**MSE**	**CPU time(s)**	**ISNR (dB)**	**MSE**
Gaussian noise with variance 1	TwoIST	233	62.4	18.95	141	92.3	18.3	159	119	17.9
	FISTA	157	57.9	19.0	167	84.8	18.5	157	112	18.1
	Proposed method	24.1	50.1	19.2	23.4	74.8	18.9	24.9	95.4	18.6

Table 11. Results of inpainting for Lifting-body image with different degradations.

	Method	Losing 30% of pixels			Losing 40% of pixels			Losing 50% of pixels		
		CPU time(s)	ISNR (dB)	MSE	CPU time(s)	ISNR (dB)	MSE	CPU time(s)	ISNR (dB)	MSE
Gaussian noise with variance 0.308033	TwoIST	973	4.65	31.3	808	8.34	29.9	807	12	29.1
	FISTA	871	4.81	31.1	822	7.74	30.3	820	12.5	29.3
	Proposed method	38.7	4.28	34.05	46.3	7.44	30.4	57.7	11.4	29.4
	Method	**Losing 30% of pixels**			**Losing 40% of pixels**			**Losing 50% of pixels**		
		CPU time(s)	**ISNR (dB)**	**MSE**	**CPU time(s)**	**ISNR (dB)**	**MSE**	**CPU time(s)**	**ISNR (dB)**	**MSE**
Gaussian noise with variance 1	TwoIST	888	6.17	30	923	8.35	28.8	908	14.3	27.8
	FISTA	815	5.83	30.3	817	7.49	29	1150	12	28.2
	Proposed method	193	4.68	33.2	222	5.89	29.2	219	9.43	28.9

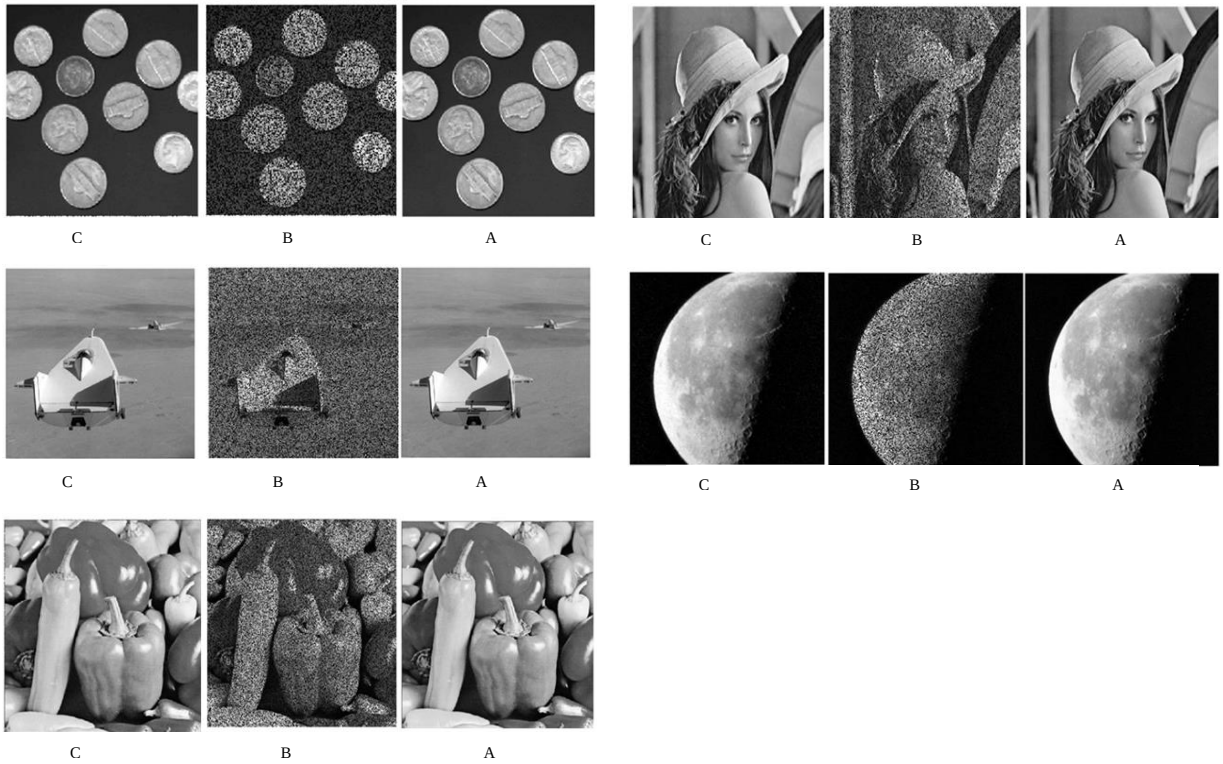

Figure 12. Results of inpainting for Coins, Lena, Moon, and Peppers: A) Original Image, B) degraded image, and C) restored image by proposed method.

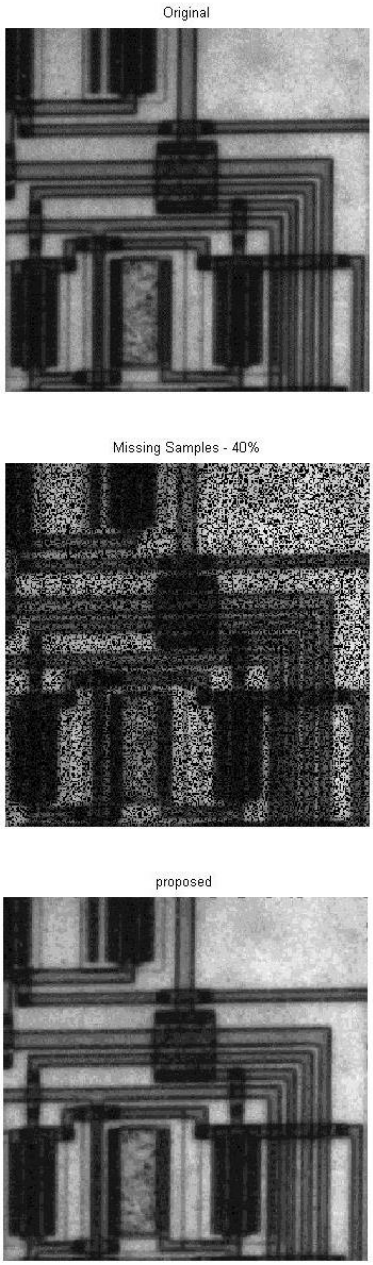

Figure 13. Results of inpainting for Cir: A) Original Image, B) degraded image, and C) restored image by proposed method.

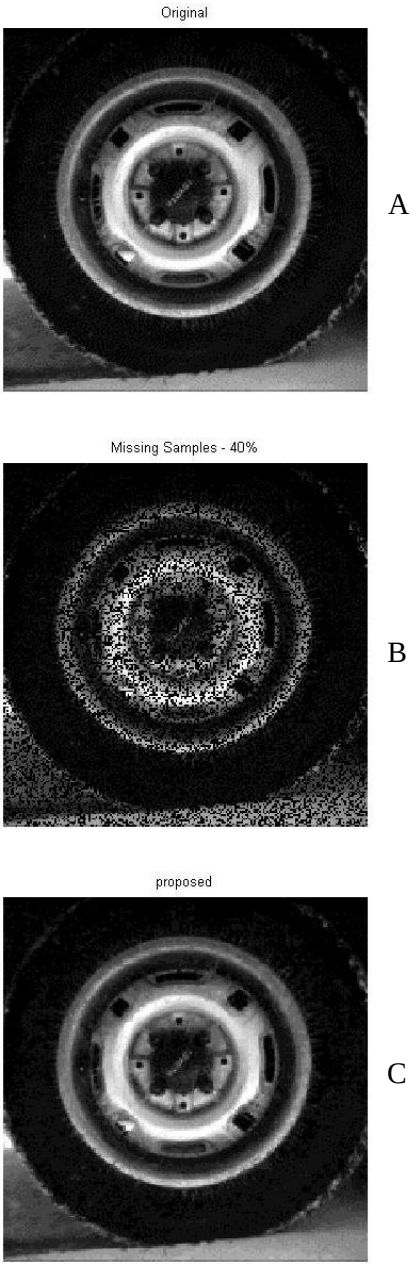

Figure 14. Results of inpainting for Tire: A) Original Image, B) degraded image, and C) restored image by proposed method.

5. Conclusions

In this paper, a new image restoration method was proposed. It used variable splitting based upon the total variant regularizer to solve the optimization problem more rapidly. In the optimization problem, since the objective function includes two terms, one term being second-order and the other one being non-linear regularizer, the variable splitting was used. This caused the argument of each term to include an individual variable. For the new optimization problem to be equal with the initial one, the undetermined optimization problem was converted to the determined one, and then the new problem was solved using the Lagrangian augmented method. Since image piecewise smoothed, traditional regularizers such as L2-norm affected restoration of edge sharpness and smooth the edges. Therefore, the total variant regularizer, due to maintaining the sharpness of the edges and removing the additive noise, was used. The image restoration was applied on two cases; deblurring/denoising and inpainting. In case of deblurring, different additive noises with

altered blurs, and for inpainting, different types of noises with different percentage of losing the pixels were used. The performance of the proposed method was compared with the TwoIST and SpaRSA methods for deblurring/denoising, and also it was compared with the FISTA and TwoIST methods for inpainting. The evaluation measures included required time for convergence (speed), ISNR, and MSE. The experimental results showed that the proposed method provided a higher ISNR, a lower MSE, and consequently, a higher quality of the restored image with higher speed of convergence compared to the TwoIST, SpaRSA, and FISTA methods for both the deblurring/denoising and inpainting cases.

References

[1] Gonzales, R. C. & Woods, R. E. (2002). Digital Image Processing, Prentice Hall.

[2] Andrews, H. & Hunt, B. (1977). Digital Image Restoration, Prentice-Hall.

[3] Chai, A. & Shen, Z. (2007). Deconvolution: A Wavelet Frame Approach. Numerische Mathematik, pp. 529–587.

[4] Dong, B. & Feng, Cai J. & Osher, S. & Shen, Z. (2012). Image Restoration: Total Variation, Wavelet frames, and beyond. Journal of the American mathematical society, vol. 25, pp. 1033-1089.

[5] Cai, J. & Chan, R. & Shen, Z. (2008). A Framelet-Based Image Inpainting Algorithm. Applied and Computational Harmonic Analysis, vol. 24, no. 3, pp. 131–149.

[6] Babacan, S. & Katsaggelos, A. & Molina, R. (2009). Variational Bayesian Blind Deconvolution Using A Total Variation Prior. IEEE Transaction Image Processing, vol. 18, no. 1, pp. 12 -26.

[7] Wang, Y. & Yin, W. & Zhang, Y. (2007). A fast algorithm for image deblurring with total variation regularization. Rice University CAAM Technical Report TR07-10, pp. 1-19.

[8] Oliveira, J. P. (2010). Advances in total variation image restoration: blur estimation, parameter and efficient optimization. Ph.D. dissertation, Inst. Superior Técnico, Univ. ontana, Missoula, MT, USA.

[9] Tiwari, P. & Dhillon, N. & Sharma, K. (2013). Analysis of Image Restoration Techniques for Developing Better Restoration Method. vol. 3, no. 4, pp. 10-14.

[10] Leung, C. M. & Lu W. S. (1993). A multiple-parameter generalization of tikhonov-miller regularization method for image restoration. Proceedings of A silomar Conf. Signals, Systems and Computers, Pacific Grove, CA, pp. 856 -860.

[11] Babacan, S. & Katsaggelos, A. & Molina, R. (2008). Parameter estimation in TV image restoration using variational distribution approximation. IEEE Trans. Image Processing, vol. 17, no. 23, pp. 326 -339.

[12] Figueiredo, A. T. & Nowak, R. D. (2003). An Em algorithm for wavelet-based image restoration. IEEE Trans. Image Processing, vol. 12, no. 8, pp. 1 -28.

[13] Bioucas-Dias, J. & Figueiredo, M. (2008). An iterative algorithm for linear inverse problems with compound regularizers. IEEE Int. Conf. Image Processing, San Diego, CA, USA, pp. 1-4.

[14] Bioucas-Dias, J. & Figueiredo, M. (2007). A new TwoIST: two-step iterative shrinkage/thresholding algorithms for image restoration. IEEE Trans. Image Processing, vol. 16, no. 12, pp. 2992 -3004.

[15] Beck, A. & Teboulle, M. (2009). A fast iterative shrinkage-thresholding algorithm for linear inverse problems. SIAM Journal of Imaging Sciences, vol. 2, pp. 183–202.

[16] Figueiredo, M. & Nowak, R. & Wright, S. (2009). Sparse Reconstruction By Separable Approximation. IEEE Trans. Image Processing, vol. 57, pp. 2479–2493.

[17] Wang, Y. & Yang, J. & Yin, W. & Zhang, Y. (2008). A New alternating minimization algorithm for total variation image reconstruction. SIAM Journal of Imaging Sciences, vol. 1, pp. 248–272.

[18] Darbon, J. & Goldfarb, D. & Osher, S. & Yin, W. (2008). Bregman iterative algorithms for l1-minimization with applications to compressed sensing. SIAM Journal of Imaging Science, vol. 1, pp. 143–168.

[19] Goldstein, T. & Osher, S. (2009). The Split bregman algorithm for l1 regularized problems. SIAM Journal of Imaging Sciences, vol. 2, no. 2, pp. 323–343.

[20] Nocedal, J. & Wright, S. J. (2006). Numerical optimization, 2nd Edition, Springer.

[21] Boyd, N. & Chu, B. & Eckstein, J. & Parikh, E. (2011). Distributed optimization and statistical learning via the alternating direction method of multipliers. Foundations and Trends in Machine Learning, vol. 3, no. 1, pp. 1-12.

[22] Maurya, A. & Tiwari, R. (2014). A Novel Method of Image Restoration by using Different Types of Filtering Techniques. International Journal of Engineering Science and Innovative Technology (IJESIT), vol. 3, no. 4, pp. 124-129.

[23] Rani, S. & Jindal, S. & Kaur, B. (2016). A Brief Review on Image Restoration Techniques. International Journal of Computer Applications, vol. 150, no. 12, pp. 30-33.

[24] Kumar, N. & Nallamothu, R. & Sethi, A. (2013). Neural Network Based Image Deblurring. Proc. of the IEEE Conference on Neural Network Applications in Electrical Engineering, 2013.

[25] Pal Singh, D. & Khare, A. (2016). Restoration of Degraded Gray Images Using Genetic Algorithm. I.J. Image, Graphics and Signal Processing, vol. 3, pp. 28-35.

[26] He, L. & Wang, Y. & Bao, C. (2016). Wavelet Frame Truncated ℓ1-regularized Image Deblurring. Proc. of the IEEE: 8th International Conference on Wireless Communications & Signal Processing (WCSP), pp. 2472-7628.

[27] Dong, W. & Zhang, L. & Shi, G. & Li, X. (2013). Nonlocally centralized sparse representation for image restoration. IEEE Transactions on Image Processing, vol. 22, no. 4, pp. 1620–1630.

[28] Dong, W. & Shi, G. & Ma, Y. & Li, X. (2015). Image Restoration via Simultaneous Sparse Coding: Where Structured Sparsity Meets Gaussian Scale Mixture. International Journal of Computer Vision.

[29] Hosseinzadeh Samani, B., HouriJafari, H. & Zareiforoush, H. (2017). Artificial neural networks, genetic algorithm and response surface methods: The energy consumption of food and beverage industries in Iran. Journal of AI and data mining, vol. 5, no. 1, pp. 79-88.

[30] Khoshdel, V. & Akbarzadeh, A. R (2016). Application of statistical techniques and artificial neural network to estimate force from sEMG signals. Journal of AI and data mining, vol. 4, no. 2, pp. 135-141.

نشریه هوش مصنوعی و داده کاوی

بازسازی تصویر با استفاده از جداسازی متغیر مبنی بر تنظیم کننده تغییرات کلی

عفت صحراگرد[1]، حسن فرسی[2،*] وسجاد محمد زاده[3]

[1] دانشکده مهندسی برق و کامپیوتر، دانشگاه بیرجند، بیرجند، ایران.

[2] دانشکده مهندسی برق و کامپیوتر، دانشگاه بیرجند، بیرجند، ایران.

[3] دانشکده فنی و مهندسی فردوس، دانشگاه بیرجند، ایران.

ارسال ۲۰۱۵/۱۱/۲۲؛ بازنگری ۲۰۱۶/۱۱/۰۵؛ پذیرش ۲۰۱۷/۰۵/۱۹

چکیده:

هدف از بازسازی تصویر، بدست‌آوردن تصویر مطلوب از تصویر خراب است. در این راستا از ترمیم که به معنی پرکردن نواحی مخدوش و از دست‌رفته تصاویر دیجیتال است استفاده می‌شود. این امر به گونه‌ای انجام می شود که برای بیننده‌ی معمولی که با تصویر اصلی آشنا نیست، قابل تشخیص نباشد. در این مقاله تصاویر ابتدا با محو شدگی و نویز و بار دیگر با از دست دادن درصدی از پیکسل‌ها، تخریب شده و سپس با روش پیشنهادی و چندین روش متداول بازسازی تصویر انجام شده است. برای بازسازی تصویر لازم است تا از روش‌های بهینه‌سازی استفاده شود. در این مقاله از روش بازسازی خطی مبتنی بر تنظیم تغییرات کلی استفاده گردیده است. متغیر مسئله‌ی بهینه‌سازی، جداسازی شده و سپس مسئله‌ی بهینه‌سازی جدید، با روش لاگرانژ افزوده حل می‌شود. آزمایش‌های انجام گرفته نشان می‌دهد که روش پیشنهادی هم در حالت حذف نویز و محو شدگی و هم در حالت ترمیم، از سایر روش‌های موجود سریع‌تر بوده و تصاویر بازسازی شده از کیفیت بهتری برخوردار می‌باشند.

کلمات کلیدی: بازسازی تصویر، ترمیم تصویر، حذف محو شدگی و نویز، تنظیم کننده‌ی تغییرات کلی، لاگرانژ افزوده.